# Infrared Imaging of Single Nanoparticles via Strong Field Enhancement in a Scanning Nanogap

A. Cvitkovic,[1,2] N. Ocelic,[1] J. Aizpurua,[3] R. Guckenberger,[2] and R. Hillenbrand[1,*]

[1]*Nano-Photonics Group, Max-Planck-Institut für Biochemie, 82152 Martinsried, Germany*
[2]*Abteilung Molekulare Strukturbiologie, Max-Planck-Institut für Biochemie, 82152 Martinsried, Germany*
[3]*Donostia International Physics Center, Paseo Manuel Lardizabal 4, 20018 Donostia-San Sebastián, Spain*

(Received 15 March 2006; published 10 August 2006)

We demonstrate nanoscale resolved infrared imaging of single nanoparticles employing near-field coupling in the nanoscopic gap between the metal tip of a scattering-type near-field optical microscope and the substrate supporting the particles. Experimental and theoretical evidence is provided that highly reflecting or polariton-resonant substrates strongly enhance the near-field optical particle contrast. Using Si substrates we succeeded in detecting Au particles as small as 8 nm ($<\lambda/1000$) at midinfrared wavelengths of about $\lambda = 10\ \mu$m. Our results open the door to infrared spectroscopy of individual nanoparticles, nanocrystals, or macromolecules.

DOI: 10.1103/PhysRevLett.97.060801 PACS numbers: 07.79.Fc, 78.67.−n, 71.36.+c

Optical antennas such as plasmon-resonant metal particles [1], engineered micro- and nanostructures [2–6], or scanning probe tips allow for efficient conversion of propagating light into nanoscale confined and strongly enhanced optical fields, and vice versa. They are therefore the key elements in the development of highly sensitive optical (bio)sensors [3], nanoscale resolution near-field optical microscopy [7–11], and infrared nanospectroscopy [12–15]. The local field enhancement can be significantly increased by optical near-field coupling of such (nano)-structures separated by a nanoscopic gap [Fig. 1(a)]. Extraordinary high optical field enhancements inside nanogaps [16] allow for single molecule Raman spectroscopy [17], two-photon excited photoluminescence [6], or white-light supercontinuum generation [4]. Further promising applications can be foreseen in near-field optical microscopy, which requires the gap fields to be scanned above the sample surface [Fig. 1(a)]. Although adequate near-field probes have been demonstrated already, their realization is a highly demanding task [5].

Here we demonstrate a simple but efficient optical microscopy concept that exploits the strong field enhancement in a scanning nanogap for highly sensitive and nanoscale resolved optical imaging. It is realized by a scattering-type near-field microscope (s-SNOM) where imaging is performed by recording light scattering from optical probes like metal nanoparticles [11] or metal tips [9,13]. Usually, the objects to be imaged are adsorbed on a low-dielectric substrate (e.g., glass) and the near-field coupling between tip and substrate is weak [Fig. 1(b)]. By employing highly reflecting substrates [Fig. 1(c)] we demonstrate that the near-field optical contrast of nanoscale objects can be strongly enhanced. This effect is explained by the strong near-field coupling between tip apex and substrate [18–20], yielding highly concentrated optical fields in the gap for probing the objects.

Near-field coupling between optical probes and flat sample surfaces has been studied in several experiments [11,12,21]. It allows optical mapping of the chemical [15,22] and structural properties [14,23] of the surface with nanoscale spatial resolution. Recently, exceptionally strong Raman signals have been observed by light scattering from a sharp metal tip probing molecules on a flat Au substrate [24]. The strong signal enhancement was explained by localized plasmon excitation in the tip-substrate cavity. Unexpected high scattering signals in near-field infrared spectroscopy of thin polymer films [15,22] and in near-field subsurface imaging [25] also indicate the importance of tip-substrate coupling.

In this Letter we apply near-field optical tip-substrate coupling to generate both strongly enhanced and confined optical fields for high-resolution near-field optical microscopy of nanoparticles. It enables for the first time infrared microscopy of single gold nanoparticles with diameters $d_{\mathrm{Au}}$ as small as 8 nm ($<\lambda/1000$) at wavelengths of about $\lambda \approx 10\ \mu$m. We note the extremely weak scattering cross section $C_{\mathrm{sca}}$ of the particles at this wavelength. It amounts to $C_{\mathrm{sca}} < 10^{-20}\ \mathrm{cm}^2$, which is 5 orders of magnitude smaller than at visible wavelengths ($C_{\mathrm{sca}} \propto d^6/\lambda^4$). Thus, infrared analysis of single nanoparticles has not been possible so far as the signals vanish far below the background level. Nevertheless, the interest to operate at infrared frequencies is motivated by the fascinating prospects of performing vibrational spectroscopy for the chemical identification of individual nanoscale objects.

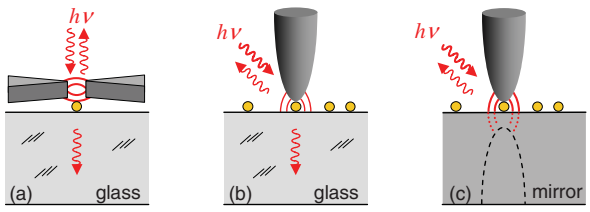


FIG. 1 (color). Optical detection of nano-objects (yellow) employing the enhanced near fields (a) in the feed gap between two antenna arms, (b) at the apex of a metal probe tip, and (c) in the gap formed between a probe tip and a highly reflecting substrate.

 

Our s-SNOM is an atomic force microscope (AFM) where a frequency-tunable infrared $CO_2$-laser beam is focused onto a Pt-coated Si tip [13]. We operate the AFM in tapping mode (tip vibration at frequency $\Omega$) to modulate the distance between tip and sample, $d = d_0 + \Delta z(1 + \cos(\Omega t))$, and thus their optical near-field coupling. The smallest distance during the tapping cycle is defined as gap width $d_0$. In combination with (i) interferometric measurement of the backscattered light and (ii) demodulation of the detector signal at $n\Omega$ (demodulation order $n > 1$) we achieve background-free recording of the near-field scattering. Phase modulation of the reference beam allows unambiguous separation of amplitude $s_n$ and phase $\varphi_n$ signals [26]. For the presented experiments third harmonic demodulation ($n = 3$) was applied.

For a first series of experiments single Au nanoparticles were immobilized by a 1 nm thick bovine serum albumine (BSA) layer on a well-polished 6H-SiC crystal that is partly covered with a 25 nm thick Au film [Fig. 2(a)]. This kind of substrate provides a wide range of dielectric constants $\varepsilon$ within the spectral region of our $CO_2$ lasers ($9\ \mu\text{m} < \lambda < 11\ \mu\text{m}$). While the Au surface represents a nearly perfectly conducting mirror ($\varepsilon_{\text{Au}} \approx -5000 + 1000i$ [27]) the dielectric value of SiC can be tuned via the laser frequency from $\varepsilon_{\text{SiC}} \approx -5$ to $\varepsilon_{\text{SiC}} \approx 3$. To prove the near-field optical origin of the detected signals, we performed 3D scanning of the substrate. In the $x$-$y$ direction the sample is scanned as usual in tapping-mode AFM. However, at every pixel we additionally retract and approach the substrate in the $z$ direction. This procedure is changing the gap width $d_0$ to verify the absence of possible artifacts that can be induced by residual background signals [13], vertical movement of the tip relative to the substrate [7], or nonlinear mechanical interactions between tip and sample [28].

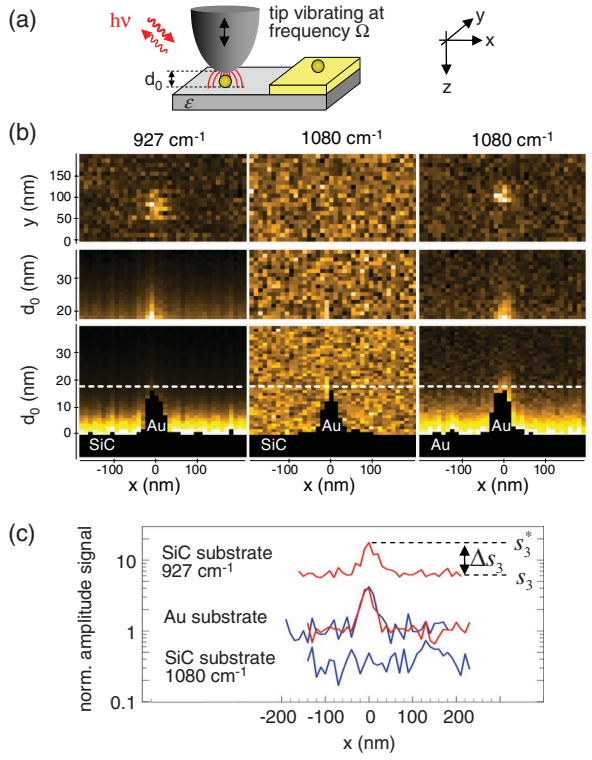


FIG. 2 (color). (a) Schematics of the experimental setup. The tip is vibrating vertically with constant amplitude $\Delta z$, while the substrate covered with Au particles is scanned in the $x$, $y$, and $z$ directions. (b) Optical amplitude images ($s_3$) of 16 nm Au particles extracted from 3D data sets. Third row: Vertical slices showing the optical signal amplitude $s_3$ dependent on the gap width $d_0$ and the horizontal particle position. The black base thereby visualizes the topography, i.e., positions where the vibrating tip comes into contact with the surface. Second row: Upper parts of the vertical slices but displayed at enhanced image contrast. First row: Horizontal slices ($x$-$y$) at distance $d_0 = 17$ nm to the substrate, i.e., 1 nm above the particle (marked by the dashed line). (c) Normalized signal amplitudes along the dashed lines in (b): blue, 1080 $\text{cm}^{-1}$; red, 927 $\text{cm}^{-1}$.

We recorded 3D data sets from single Au particles ($d_{\text{Au}} \approx 16 \pm 0.5$ nm) adsorbed on either the Au or the SiC surface, at 1080 $\text{cm}^{-1}$ ($\varepsilon_{\text{SiC}} \approx 3$, weak dielectric substrate) and at 927 $\text{cm}^{-1}$ ($\varepsilon_{\text{SiC}} \approx -2$, phonon-polariton-resonant near-field coupling between tip and SiC [12]). The laser power applied to the tip (1.5 mW) was kept constant during all measurements. We validate the near-field optical origin of the data sets by extracting vertical $s_3$ images, i.e., slices perpendicular to the surface [Fig. 2(b), third row]. The images clearly show that significant signal amplitudes $s_3$ (bright pixels) are measured only within the range of near-field interaction, i.e., for tip-surface distances that are on the scale of the probe radius ($r \approx 25$ nm) [8,13]. From the 3D data sets we can also extract constant height slices [Fig. 2(b), first row] corresponding to scanning the Au particles with fixed gap width $d_0$ (tip-substrate distance). The images obtained for particles on the Au mirror reveal a bright spot with a FWHM of about 40 nm($= \lambda/250$). Obviously, the presence of the Au particle increases the signal amplitude $s_3$. Similar images are obtained for the SiC substrate at 927 $\text{cm}^{-1}$. However, at 1080 $\text{cm}^{-1}$, where the dielectric value of the SiC substrate is low ($\varepsilon_{\text{SiC}} \approx 3$), we do not observe a significant optical signal either above the SiC surface or above the Au particle.

For a quantitative analysis we extract line plots from Fig. 2(b) at positions marked by the dashed lines ($d_0 = 17$ nm) and display them in Fig. 2(c). The results are normalized to the signal amplitude obtained for the empty gap formed between tip and Au substrate ($d_0 = 17$ nm). We find that both the signal amplitude $s_3^*$ and the absolute optical particle contrast $\Delta s_3 = s_3^* - s_3$ are enhanced when replacing the weak dielectric SiC (1080 $\text{cm}^{-1}$) by the Au surface. Here $s_3^*$ is the signal amplitude 1 nm above the particle and $s_3$ the signal amplitude for the empty gap ($d_0 = 17$ nm). An even further threefold enhancement of $\Delta s_3$ is observed for the SiC substrate at 927 $\text{cm}^{-1}$. As reported earlier [12,18,19], at this frequency the near fields at the probe apex can excite phonon polaritons in SiC.

They cause a resonant near-field interaction such that the signal amplitudes $s_3$ and $s_3^*$ are larger than on the Au substrate. Altogether, the line plots in Fig. 2(c) clearly demonstrate the two essential observations of our work. First, the scattering signals increase when a small Au particle is placed in the gap between tip apex and substrate. Second, the absolute optical particle contrast $\Delta s_3 = s_3^* - s_3$ can be significantly enhanced by employing metal or polariton-resonant substrates.

An important consequence of substrate-enhanced near-field imaging is the higher contrast-to-noise ratio. However, as seen in Fig. 2(c), the absolute noise level increases in our experiments with higher signal amplitudes. This is mainly due to the strongly distance dependent near-field coupling [Fig. 2(b)] which translates mechanical vibrations into the optical noise. Consequently, even better contrast-to-noise ratios could be achieved with a mechanically more stable setup.

In our second experiment we study how $\Delta s_3$ depends on the particle size. For this purpose Au particles ($6\ \text{nm} < d_{\text{Au}} < 20\ \text{nm}$) are adsorbed onto a Si substrate. We use Si as it offers a smooth and highly reflecting surface ($\varepsilon \approx 11.7$ [27]) in a broad spectral region, which is important for infrared spectroscopy of nanoparticles. We determine the optical particle contrast $\Delta s_3 = s_3^* - s_3$ by measuring (i) the signal amplitude $s_3$ above various particles of different diameters $d_{\text{Au}}$ and (ii) the signal amplitude $s_3$ above the flat Si surface as a function of $d_0$ [Fig. 3(a)]. The latter measurement (blue dots) yields a typical approach curve $s_3(d_0)$ [13]. With decreasing gap width $d_0$ the near-field interaction between probe and surface is increasing, and thus the scattered signal amplitude $s_3$ increases as well. When a particle of diameter $d_{\text{Au}} = d_0$ is located inside the gap, we find the signal amplitude $s_3^*$ (red symbols) clearly enhanced over $s_3$, in accordance with Fig. 2(c). The red symbols in Fig. 3(a) exhibit a significant optical contrast $\Delta s_3$ above the measurement error for all particles down to $d_{\text{Au}} = 8\ \text{nm}$.

We can explain the approach curve $s_3(d_0)$ on Si [Fig. 3(a), blue dots] by describing the probe by a dipole $p$. The scattered signal amplitude $s_3$ is calculated from quasielectrostatic near-field interaction between the probe dipole $p$ and its image $p' = \beta p$ in the flat substrate [13]. The strength of the image dipole is thereby given by the surface response function $\beta = (\varepsilon - 1)/(\varepsilon + 1)$. For the polarizability of the probe dipole $p$ we assume that of a metal ellipsoid [1] with a tip radius $r = 25\ \text{nm}$ derived from topography images. Fitting the experimental approach curve $s_3(d_0)$ by our model we obtain the semimajor axis $a = 46\ \text{nm}$ and a good quantitative agreement between experiment and theory. Note that the model takes into account tip vibration ($\Delta z = 25\ \text{nm}$) and signal demodulation at $n = 3$.

The modified signal amplitude $s_3^*$ (Au particle inside the gap) is obtained from calculating the electrostatic near-field coupling between probe dipole $p$, particle dipole $p_{\text{Au}}$, and the corresponding image dipoles $p'$ and $p'_{\text{Au}}$ [29]

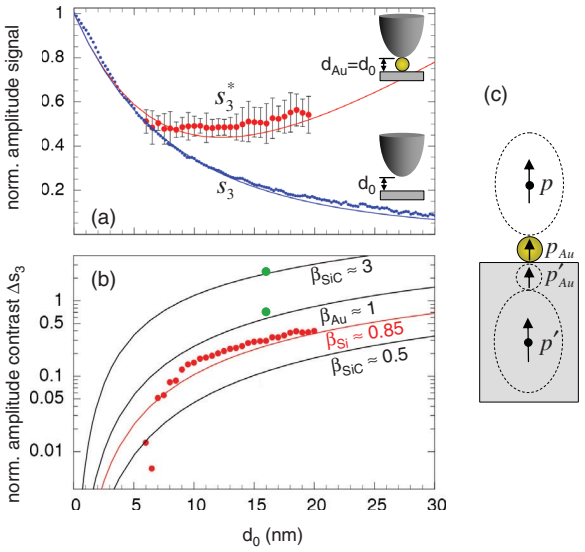


FIG. 3 (color). (a) Experimental (dots) and theoretical (solid lines) optical signal amplitudes $s_3$ and $s_3^*$ as a function of the gap width $d_0 = d_{\text{Au}}$. Each $s_3^*$ value (red symbols) represents an average obtained from more than 10 Au particles of diameter $d_{\text{Au}} \pm 0.25$ nm. (b) Absolute optical particle contrast $\Delta s_3 = s_3^* - s_3$ for different substrates. The experimental $\Delta s_3$ values (red symbols) for the Si substrate are taken from (a) and that for the 16 nm Au particles (green symbols) from Fig. 2(c). The solid lines show dipole calculations applying the same parameters as in (a) but different dielectric values for the substrate. No further fitting was performed. All values are normalized to the $s_3$ value on the Si substrate at $d_0 = 0$. (c) Illustration of the dipole model.

[Fig. 3(c)]. The particle dipole thereby is given by the polarizability of a Au sphere, $\alpha_{\text{Au}} \approx 4\pi\varepsilon_0 d_{\text{Au}}^3$, with diameter $d_{\text{Au}} = d_0$. As seen in Fig. 3 the theoretical results (red solid lines) obtained for $s_3^*$ and $\Delta s_3 = s_3^* - s_3$ show a good agreement with the experimental data (red symbols). $s_3^*$ exceeds $s_3$ due to the presence of a new center of polarization ($p_{\text{Au}}$) inside the gap that couples to the probe and image dipole, thereby increasing both the near-field coupling of the entire dipole system and the near fields in the gap region. It is also found that $\Delta s_3$ is decreasing for smaller particles. We note the important fact that $\Delta s_3$ does not scale with the polarizability ($\propto d_{\text{Au}}^3$) of the particles like the scattered field from isolated spheres. Decreasing the particle size from 20 nm to 10 nm the particle contrast $\Delta s_3$ is reduced by only a factor of 3 rather than by a factor of 8. This advantageous behavior can be explained by the increased near-field coupling between tip and substrate when the particle size, i.e., the gap width $d_0 = d_{\text{Au}}$, is decreased. The enhanced near-field coupling provides higher fields for polarizing the reduced amount of matter inside the gap. Thus it partially compensates the decreasing particle polarizability.

Repeating the calculation for a Au and a SiC substrate we can compare the dipole model also with experimental results (green symbols) extracted from Fig. 2(c). With increasing strength $\beta$ of the mirror dipole the enhanced near-field coupling yields a higher polarization of the gold

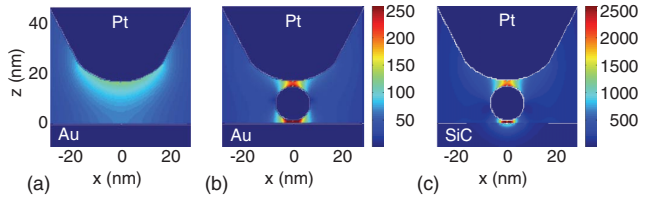


FIG. 4 (color). (a) Field distribution in the gap between a Pt cone (25 nm tip radius) and a Au surface at frequency 927 $cm^{-1}$. (b) Au particle of 16 nm inside the gap. (c) Tenfold near-field enhancement in case of a phonon-polariton-resonant SiC substrate. (a)–(c) All values depict the electric field amplitudes normalized to the illuminating field. The 1 nm gap between particle and substrate accounts for the BSA layer in the experiment. As we operate our microscope in tapping mode, we assume that the smallest tip-particle distance during the tapping cycle is about 1–2 nm. Latter value is chosen for the calculations.

particle and thus an enhanced amplitude contrast $\Delta s_3$. We note the good agreement between experimental and calculated signal amplitudes, although the dipole model neglects higher multipole excitations, retardation, and radiation damping. To provide a more exact description of enhanced near-field coupling in the tip-substrate gap, we perform a full electrodynamic calculation for 927 $cm^{-1}$ using the boundary element method [30]. We first calculate the near-field distribution for a Pt tip above a Au surface showing field concentration at the tip apex [Fig. 4(a)]. Because of the near-field coupling with the Au mirror, the fields are enhanced by a factor of 4 compared to an isolated tip. In case a Au particle is placed inside the gap, the fields increase by another factor of 5 [Fig. 4(b)]. The main spots of enhancement are thereby located at the particle-substrate and particle-tip junctions. Replacing the Au substrate by SiC the excitation of phonon-polaritons in the SiC further increases the near-field coupling, which additionally enhances the fields by a factor of about 10 [Fig. 4(c)]. While these results support our conclusions drawn from the dipole model, higher multipoles and the geometry of the particle junctions yield both a stronger field confinement and field enhancement in the exact calculation. The latter reaches values comparable with that of plasmon-resonant nanolenses formed by self-similar particle chains [16] and will be an interesting topic for further studies.

In conclusion, we demonstrated that tip-substrate coupling in s-SNOM enables nanoscale resolved infrared imaging of particles even below 10 nm in diameter. We showed that the near-field optical particle contrast can be strongly enhanced by highly reflecting substrates such as Au and Si. Particularly strong particle contrasts are achieved by resonant near-field coupling provided by phonon-polariton excitation in a SiC substrate. Our results already promise a wide application potential in high-resolution imaging of nanoscale objects (e.g., gold biolabels) and in infrared near-field spectroscopy of thin films [15] and organic as well as biological nanoparticles [31]. We expect further improvement of the probe sensitivity by employing resonant and sharper probe tips, which could open the door to infrared spectroscopy of even single molecules at ultrahigh spatial resolution. Finally, by exploiting plasmon-polariton excitation in metal substrates [24] the demonstrated effect could also push the limits in tip-enhanced spectroscopy at visible frequencies [9].

The authors thank O. Medalia and M. Beck for providing gold nanoparticles, F. J. García de Abajo for calculation software, and F. Keilmann, T. Taubner, and N. Issa for fruitful discussions. Supported by BMBF Grant no. 03N8705, DFG, and Nanotron Etortek project.

*Electronic address: hillenbr@biochem.mpg.de

[1] U. Kreibig and M. Vollmer, *Optical Properties of Metal Clusters* (Springer-Verlag, Berlin, 1995).
[2] K. B. Crozier *et al.*, J. Appl. Phys. **94**, 4632 (2003).
[3] W. L. Barnes, A. Dereux, and T. W. Ebbesen, Nature (London) **424**, 824 (2003).
[4] P. Mühlschlegel *et al.*, Science **308**, 1607 (2005).
[5] J. N. Farahani *et al.*, Phys. Rev. Lett. **95**, 017402 (2005).
[6] P. J. Schuck *et al.*, Phys. Rev. Lett. **94**, 017402 (2005).
[7] H. F. Hamann, A. Gallagher, and D. J. Nesbitt, Appl. Phys. Lett. **73**, 1469 (1998).
[8] R. Hillenbrand and F. Keilmann, Phys. Rev. Lett. **85**, 3029 (2000).
[9] A. Hartschuh *et al.*, Phys. Rev. Lett. **90**, 095503 (2003).
[10] H. G. Frey *et al.*, Phys. Rev. Lett. **93**, 200801 (2004).
[11] T. Kalkbrenner *et al.*, Phys. Rev. Lett. **95**, 200801 (2005).
[12] R. Hillenbrand, T. Taubner, and F. Keilmann, Nature (London) **418**, 159 (2002).
[13] F. Keilmann and R. Hillenbrand, Phil. Trans. R. Soc. A **362**, 787 (2004).
[14] N. Ocelic and R. Hillenbrand, Nat. Mater. **3**, 606 (2004).
[15] T. Taubner, R. Hillenbrand, and F. Keilmann, Appl. Phys. Lett. **85**, 5064 (2004).
[16] L. Kuiru, M. I. Stockman, and D. J. Bergman, Phys. Rev. Lett. **91**, 227402 (2003).
[17] H. Xu *et al.*, Phys. Rev. Lett. **83**, 4357 (1999).
[18] P. K. Aravind and H. Metiu, Surf. Sci. **124**, 506 (1983).
[19] J. Renger *et al.*, Phys. Rev. B **71**, 075410 (2005).
[20] F. Le *et al.*, Nano Lett. **5**, 2009 (2005).
[21] T. Taubner, F. Keilmann, and R. Hillenbrand, Nano Lett. **4**, 1669 (2004).
[22] M. B. Raschke *et al.*, Chem. Phys. Chem. **6**, 2197 (2005).
[23] A. Huber *et al.*, Nano Lett. **6**, 774 (2006).
[24] B. Pettinger *et al.*, Phys. Rev. Lett. **92**, 096101 (2004).
[25] T. Taubner, F. Keilmann, and R. Hillenbrand, Opt. Express **13**, 8893 (2005).
[26] N. Ocelic, A. Huber, and R. Hillenbrand, Appl. Phys. Lett. (to be published).
[27] E. W. Palik, *Handbook of Optical Constants of Solids* (Academic Press, San Diego, 1985).
[28] A. Bek, R. Vogelgesang, and K. Kern, Appl. Phys. Lett. **87**, 163115 (2005).
[29] V. V. Gozhenko, L. G. Grechko, and K. W. Whites, Phys. Rev. B **68**, 125422 (2003).
[30] F. J. Garcia de Abajo and A. Howie, Phys. Rev. Lett. **80**, 5180 (1998).
[31] M. Brehm *et al.*, Nano Lett. **6**, 1307 (2006).